

Theory of the critical current in two-band superconductors with application to MgB₂

E.J. Nicol*

Department of Physics, University of Guelph, Guelph, Ontario, N1G 2W1, Canada

J.P. Carbotte[†]

Department of Physics and Astronomy, McMaster University, Hamilton, Ontario, L8S 4M1, Canada

(Dated: November 21, 2018)

Using a Green's function formulation of the superfluid current j_s , where a momentum q_s is applied to the Cooper pair, we have calculated j_s as a function of q_s , temperature, and impurity scattering for a two-band superconductor. We consider both renormalized BCS and full strong-coupling Eliashberg theory. There are two peaks in the current as a function of q_s due to the two energy scales for the gaps and this can give rise to non-standard behavior for the critical current. The critical current j_c , which is given as the maximum in j_s , can exhibit a kink as a function of temperature as the maximum is transferred from one peak to other. Other temperature variations are also possible and the universal BCS behavior is violated. The details depend on the material parameters of the system, such as the amount of coupling between the bands, the gap anisotropy, the Fermi velocities, and the density of states of each band. The Ginzburg-Landau relation between j_c , the penetration depth λ_L and thermodynamic critical field H_c , is modified. Using Eliashberg theory with the electron-phonon spectral densities given from bandstructure calculations, we have applied our calculations for j_s and j_c to the case of MgB₂ and find agreement with experiment.

PACS numbers: 74.20-z,74.70.Ad,74.25.Fy,74.25.Sv

I. INTRODUCTION

Two-band superconductivity was first proposed in the late 1950's and further studied in the 1960's and 1970's as a possible explanation for understanding superconductivity in s- and d- band metals. However, it was not until the discovery of superconductivity at relatively high temperature in MgB₂ in 2001, that the most promising example of two-band superconductivity was found. After nearly four years of effort and the development of an extensive literature based on this material, it is now evident that this compound is an electron-phonon mediated superconductor, but with two distinct bands and hence two energy gaps. Indeed, this is firmly established from detailed bandstructure calculations that provide the electron-phonon spectral densities which, when in turn are used in a two-band Eliashberg formalism, give rise to predictions which are in accord with experiment. In fact, the picture that emerges is one of excellent agreement with the data, with the match being as good as is found between theory and experiment in conventional one-band superconductors[1]. A detailed review and summary of the level of agreement found for the thermodynamic properties, BCS ratios, penetration depth and temperature-dependent energy gaps is found in Ref. [2]. With such an extensive comparison between rigorous Eliashberg theory and experiment completed, it is now appropriate to move on to the transport properties where less theoretical work has been done.

In this paper, we consider the critical current which is of fundamental interest in the discussion of transport. While most technological applications focus on the bulk critical current density, which requires understanding of flux lattice pinning, etc., here we are presenting the critical current in thin films. This geometry is more relevant to understanding issues associated with the fundamental superconducting state, rather than focussing on material details that lead to vortex pinning, etc., and hence can be expected to provide further insight into the nature of multiband superconductivity in these materials. We note in passing, at this point, that some authors use the term depairing current for the critical current although, technically, the depairing current is the current at which the first Cooper pair is broken and the gap decreases, and the critical current is the maximum current possible, which is greater than the depairing current. In simple one-band s-wave BCS theory the values are almost the same and hence there is the tendency to use the terms interchangeably. Here, these two quantities can be quite different and so we will use the term critical current to refer to the global maximum obtainable in the current density.

The full temperature-dependence of the critical current j_c was first studied in conventional one-band s-wave BCS superconductors by Rogers[3] and Bardeen[4]. Further work following on this was done by Parameter[5] for the clean limit, and by Maki[6, 7] for the dirty limit, where the latter author introduced a description of the superfluid current density using the Green's function formalism. A study of the effect of a current on the quasiparticle states density of states of a superconductor was done by Fulde[8]. The most general work was that of Kupriyanov and Lukichev[9], who calculated the full temperature dependence of the critical current in BCS

*Electronic address: nicol@physics.uoguelph.ca

[†]Electronic address: carbotte@mcmaster.ca

theory for arbitrary impurity scattering, which returned the usual Ginzburg-Landau results for the critical current near T_c [10]. Further considerations led to an initial attempt to include strong inelastic scattering[11] followed by a full Eliashberg calculation and study of strong coupling effects for conventional electron-phonon superconductors done by ourselves[12]. Thus, the formalism and basic one-band results have been well-established in both the weak-coupling BCS limit and strong-coupling Eliashberg regime, at all temperatures and for arbitrary impurity scattering.

More recently there has been a renewed theoretical effort on the critical current as applied to exotic gaps, which are anisotropic, such as d-wave[13, 14] and f-wave[14, 15]. The two-band case is, in some sense, a highly anisotropic system and hence the study of the critical current in this instance also complements these recent works.

With regard to MgB₂, specifically, there has been some recent experimental work by Kunchur[16], where the critical current has been measured in these systems. On the theoretical side, Koshelev and Golubov[17] have gone beyond Ginzburg-Landau to use the Usadel equations to study this system and find interesting effects such as a kink in the temperature-dependence of the c-axis critical current that reflects the underlying two-band nature. This type of feature is observed in other properties such as the penetration depth which also shows an inflection point in the temperature dependence, however, these effects may disappear with increased interband coupling. Finally, a more recent work has been done on the topic of the non-linear term in the superfluid current in MgB₂ and its effect on the nonlinear microwave response, which is relevant for device applications[18].

In our work here, we use the general Green's function formulation presented by Maki[7] where the Cooper pairs are given a finite center of mass momentum q_s . This q_s leads to a boost in the quasiparticle energy (sometimes called a Doppler shift). The superfluid velocity $v_s = q_s/m$ is taken as uniform in the case of discussing currents in thin films or wires, unlike the Doppler shift effect in the context of superfluid currents in the vortex state, where v_s varies with spatial position. This latter topic has been the subject of a large number of papers in the recent literature relating to d-wave superconductors[19].

A very fine physical description of the effect of this Doppler shift on the quasiparticle density of states and the resulting effect on the superfluid density is presented in a paper by Xu et al.[20], where they consider the non-linear Meissner effect in d-wave superconductors from a starting point that discusses the basics of the superfluid current density.

Thus, with a body of literature developing on the topic of critical currents and superfluid currents, it is of interest to elucidate the features in the critical current due to two-band superconductivity, where unusual effects can occur due to a transfer from one band to the other of the dominant contribution to superfluid current and hence

the critical current.

Our paper is structured in the following manner. In Section II, we introduce the basic theoretical equations which we have evaluated. We then examine, in Section III, results for renormalized BCS theory near T_c and at $T = 0$ and apply these results to MgB₂. In Section IV, we present our Eliashberg results for finite temperature and with impurities, evaluating the critical current for MgB₂ and other model parameters. We also compare our results to the data for MgB₂. Finally, we form our conclusions in Section V.

II. THEORY

While various approaches have been used in the past for calculating the superfluid current, we will use the Green's function method as presented by Maki[7]. Thus the superfluid current density \vec{j}_s is given in terms of finite temperature Green's functions as:

$$\vec{j}_s = \frac{eT}{m} \sum_{n=-\infty}^{\infty} \int \frac{d^3p}{(2\pi)^3} \text{Tr}[\vec{p} G_{\omega_n, \vec{q}_s}(\vec{p})] \quad , \quad (1)$$

where e is the electron charge, m , the electron mass, $\vec{p} = m\vec{v}$ is the electron momentum, and T is the temperature. The Green's function is given in terms of the Matsubara representation by

$$G_{\omega_n, \vec{q}_s}(\vec{p}) = [i\tilde{\omega}(n) - \vec{v} \cdot \vec{q}_s + \xi\rho_3 + \tilde{\Delta}(n)\rho_1\sigma_2]^{-1}, \quad (2)$$

where $\xi = p^2/2m - \mu$, μ is the chemical potential, and the ρ_i and σ_i are the Pauli matrices for the particle-hole and spin spaces, respectively. The \vec{q}_s is the applied superfluid momentum and it results in a shift of the quasiparticle energies, given to first order in q_s by $\vec{v} \cdot \vec{q}_s$. Here, $\tilde{\Delta}(n)$ and $\tilde{\omega}(n)$ are the imaginary axis renormalized superconducting order parameter and renormalized Matsubara frequencies, respectively, and are defined below.

The integral over energy ξ for the combined Eqns. (1) and (2) can be done and the result, generalized to two bands, is given in terms of a sum of two partial currents j_{s1} and j_{s2} , for the first and second band, respectively:

$$\vec{j}_s = \vec{j}_{s1} + \vec{j}_{s2} \quad (3)$$

with

$$j_{si} = \frac{3en_i}{mv_{Fi}} \pi T \sum_{n=-\infty}^{+\infty} \int_{-1}^1 dz \frac{i(\tilde{\omega}_i(n) - is_i z)z}{\sqrt{(\tilde{\omega}_i(n) - is_i z)^2 + \tilde{\Delta}_i^2(n)}}, \quad (4)$$

where $s_i = v_{Fi}q_s$, n_i is the electron density and v_{Fi} is the Fermi velocity of the i 'th band ($i = 1, 2$). The non-linear Eliashberg equations for $\tilde{\Delta}_i(n) = Z_i(n)\Delta_i(n)$ and $\tilde{\omega}_i(n) = Z_i(n)\omega_n$ have been generalized to two bands and with the inclusion of the effect of the q_s , they are given

as[2, 12]:

$$\begin{aligned}\tilde{\Delta}_i(n) &= \pi T \sum_m \sum_j [\lambda_{ij}(m-n) - \mu_{ij}^*(\omega_c)\theta(\omega_c - |\omega_m|)] \\ &\times \int_{-1}^1 \frac{dz}{2} \frac{\tilde{\Delta}_j(m)}{\sqrt{(\tilde{\omega}_j(m) - is_j z)^2 + \tilde{\Delta}_j^2(m)}} \\ &+ \pi \sum_j (t_{ij}^+ - t_{ij}^-) \int_{-1}^1 \frac{dz}{2} \frac{\tilde{\Delta}_j(n)}{\sqrt{(\tilde{\omega}_j(n) - is_j z)^2 + \tilde{\Delta}_j^2(n)}}\end{aligned}\quad (5)$$

and

$$\begin{aligned}\tilde{\omega}_i(n) &= \omega_n + \pi T \sum_m \sum_j \lambda_{ij}(m-n) \\ &\times \int_{-1}^1 \frac{dz}{2} \frac{\tilde{\omega}_j(m) - is_j z}{\sqrt{(\tilde{\omega}_j(m) - is_j z)^2 + \tilde{\Delta}_j^2(m)}} \\ &+ \pi \sum_j (t_{ij}^+ + t_{ij}^-) \int_{-1}^1 \frac{dz}{2} \frac{\tilde{\omega}_j(n) - is_j z}{\sqrt{(\tilde{\omega}_j(n) - is_j z)^2 + \tilde{\Delta}_j^2(n)}},\end{aligned}\quad (6)$$

where $t_{ij}^+ = 1/(2\pi\tau_{ij}^+)$ and $t_{ij}^- = 1/(2\pi\tau_{ij}^-)$ are the ordinary and paramagnetic impurity scattering rates, respectively, and the electron-phonon kernels $\alpha_{ij}^2 F(\Omega)$ with phonon energy Ω enter through

$$\lambda_{ij}(m-n) \equiv 2 \int_0^\infty \frac{\Omega \alpha^2 F_{ij}(\Omega)}{\Omega^2 + (\omega_n - \omega_m)^2} d\Omega. \quad (7)$$

Here, the n indexes the n 'th Matsubara frequency ω_n , with $\omega_n = (2n-1)\pi T$, where $n = 0, \pm 1, \pm 2, \dots$. The μ_{ij}^* are Coulomb repulsions, with a high energy cutoff ω_c usually taken to be about six to ten times the maximum phonon frequency. As written, Eqns. (4)-(6) are for three dimensions with isotropic Fermi surface. For general anisotropic Fermi surface, a Fermi surface integral would remain, which would need to be done numerically[18]. This goes beyond the scope of this paper, however, such details are not expected to change the qualitative features of our results but rather lead to quantitative changes only.

In the following sections, we present both Eliashberg results and renormalized BCS (RBCS) results, the latter of which can be quite successful at capturing the essential features of the Eliashberg calculations without the full numerical complications of the more sophisticated calculations even for two-band models[2]. To develop the RBCS results we use the two-square-well approximation or $\lambda^{\theta\theta}$ model written for two-bands (for details see Ref. [2]), where now

$$\Delta_i(T) = \frac{\pi T}{Z_i} \sum_{m, |\omega_m| < \omega_D} \sum_j \int_{-1}^1 \frac{dz}{2} \frac{[\lambda_{ij} - \mu_{ij}^*] \Delta_j(T)}{\sqrt{(\omega_m - is_j z)^2 + \Delta_j^2}}. \quad (8)$$

In this expression, $\bar{s}_j = s_j/Z_j$,

$$\lambda_{ij} = 2 \int_0^\infty \frac{\alpha^2 F_{ij}(\Omega)}{\Omega} d\Omega \quad (9)$$

and

$$Z_i = 1 + \sum_j \lambda_{ij}, \quad (10)$$

with ω_D taken to represent either the Debye frequency or some other characteristic energy scale representing the phonons in the system. Likewise, the current from Eq. (4) can be reduced to

$$j_{si} = \frac{3en_i}{mv_{Fi}} \pi T \sum_{n=-\infty}^{+\infty} \int_{-1}^1 dz \frac{i(\omega_n - i\bar{s}_i z)z}{\sqrt{(\omega_n - i\bar{s}_i z)^2 + \Delta_i^2(T)}}. \quad (11)$$

Equations (8) and (11) will be used in the next section to develop analytic results for comparison with full numerical calculation.

III. RENORMALIZED BCS RESULTS

A. RBCS near T_c

In order to evaluate the critical current near T_c , we need to know the effect of the current on the gap near T_c . In this limit, both Δ and q_s will be small. After long but straightforward algebra, to first order in $(1-t)$ where $t = T/T_c$ is the reduced temperature, the gap equation of Eq. (8) reduces to the form

$$1 = \bar{\lambda}_{11} F_1 + \frac{\bar{\lambda}_{12}\bar{\lambda}_{21}}{1 - \bar{\lambda}_{22}F_2} F_1 F_2 + \Delta_1^2 G(T_c) H_1, \quad (12)$$

with a second equation obtained from Eq. (12) by switching indices $1 \leftrightarrow 2$. Here

$$\bar{\lambda}_{ij} = \frac{\lambda_{ij} - \mu_{ij}^*}{Z_i} \quad (13)$$

and

$$F_i \equiv F_i(T) = \ln\left(\frac{1.13\omega_D}{T}\right) + \frac{2}{3} G(T) v_{Fi}^* q_s^2, \quad (14)$$

where $v_{Fi}^* \equiv v_{Fi}/(1 + \lambda_{ii} + \lambda_{ij})$ and $G(T) = -7\zeta(3)/8(\pi T)^2$. For $\Delta_1(T) \rightarrow 0$ as $T \rightarrow T_c$ and with no superfluid momentum ($q_s = 0$), we recover the equation for the critical temperature (symmetric in $1 \leftrightarrow 2$)[2]:

$$1 = (\bar{\lambda}_{11} + \bar{\lambda}_{22})g + (\bar{\lambda}_{12}\bar{\lambda}_{21} - \bar{\lambda}_{11}\bar{\lambda}_{22})g^2, \quad (15)$$

with $g = \ln(1.13\omega_D/T_c)$. Throughout this paper, we will find it instructive to consider several simplifying limiting cases. The completely decoupled case corresponds to $\lambda_{12} = \lambda_{21} = 0$ and the assumption that $\bar{\lambda}_{11} > \bar{\lambda}_{22}$. In

this case, the first channel determines the T_c , which is given by $1.13\omega_D \exp(-1/\bar{\lambda}_{11})$. As an aside, we note that the small separable a^2 anisotropy model studied extensively in the older literature[23] maps on to this model if $\bar{\lambda}_{11} = \bar{\lambda}(1+a)^2/2$, $\bar{\lambda}_{22} = \bar{\lambda}(1-a)^2/2$ and $\bar{\lambda}_{12}\bar{\lambda}_{21} = \bar{\lambda}(1-a^2)/2$, with the anisotropy a^2 assumed small. In this case, Eq. (15) simplifies greatly since $\bar{\lambda}_{12}\bar{\lambda}_{21} = \bar{\lambda}_{11}\bar{\lambda}_{22}$ so that $g = 1/(\bar{\lambda}_{11} + \bar{\lambda}_{22}) = 1/[\bar{\lambda}(1+a^2)] = (1+\lambda)/[\lambda(1+a^2)]$ which gives $T_c = 1.13\omega_D \exp(-(1+\lambda)/[\lambda(1+a^2)])$. This is the well-known result that anisotropy increases the value of the critical temperature over its isotropic value ($a^2 = 0$).

Returning to Eq. (12) which gives the gap just below T_c , we need to specify H_i . It is given (after more lengthy algebra) as

$$H_1 = \bar{\lambda}_{11} + \frac{g\bar{\lambda}_{12}\bar{\lambda}_{21}}{1-g\bar{\lambda}_{22}} \left\{ 1 + \frac{g^2\bar{\lambda}_{21}^2}{(1-g\bar{\lambda}_{22})^3} \right\} \quad (16)$$

and an equivalent expression for H_2 is obtained from Eq.(16) by switching indices $1 \leftrightarrow 2$. Solving for $\Delta_1^2(t)$, we find

$$\Delta_1^2(t) = -\frac{(1-t)}{G(T_c)} \frac{1}{\chi_1} - \frac{2}{3} q_s^2 \frac{1}{\chi_1'}, \quad (17)$$

with

$$\frac{1}{\chi_1} = \frac{1}{H_1} \left[\bar{\lambda}_{11} + \frac{\bar{\lambda}_{12}\bar{\lambda}_{21}}{1-g\bar{\lambda}_{22}} \left(2g + \frac{g^2\bar{\lambda}_{22}}{1-g\bar{\lambda}_{22}} \right) \right] \quad (18)$$

and

$$\frac{1}{\chi_1'} = \frac{1}{H_1} \left[\bar{\lambda}_{11} v_{F1}^{*2} + \frac{g\bar{\lambda}_{12}\bar{\lambda}_{21}}{1-g\bar{\lambda}_{22}} \left(v_{F1}^{*2} + v_{F2}^{*2} + \frac{g\bar{\lambda}_{22} v_{F2}^{*2}}{1-g\bar{\lambda}_{22}} \right) \right]. \quad (19)$$

Likewise, the gap $\Delta_2(t)$, is formed from the above three equations by exchanging $1 \leftrightarrow 2$. When $q_s = 0$, these equations properly reduce to those obtained previously by Nicol and Carbotte[2]. In the limit of decoupled bands, $1/\chi_1 = 1$ and $1/\chi_1' = v_{F1}^{*2}$. Some care is required when treating the equivalent equations for $1/\chi_2$ and $1/\chi_2'$ because the combination $(1-g\bar{\lambda}_{22})$ is replaced by $(1-g\bar{\lambda}_{11})$, which is zero. Nevertheless, we can show $1/\chi_2 = 1/\chi_2' = 0$, which is expected on physical grounds as the second band does not contribute near T_c , where $\Delta_2^2(t) = 0$ for $t \rightarrow 1$, and $\Delta_1^2(t) = (1-t)8(\pi T_c)^2/[7\zeta(3)]$, a well-known result. We can also recover other well-known results for the small separable anisotropy model defined previously. Note first that when the Fermi velocities are equal, $1/\chi_1'$ in Eq. (19) reduces to v_F^{*2}/χ_1 , with $1/\chi_1$ given by Eq. (18). Further, $1/\chi_1 = (1+a)^2(1-5a^2)$ and $1/\chi_2 = (1-a)^2(1-5a^2)$ which leads to (Eq. (17))

$$\Delta_1^2(t) = (1+a)^2(1-5a^2) \left[(1-t) \frac{8(\pi T_c)^2}{7\zeta(3)} - \frac{2}{3} q_s^2 v_F^{*2} \right] \quad (20)$$

and an identical equation for the second gap with the first factor of $(1+a)^2$ replaced by $(1-a)^2$. For $q_s = 0$,

Eq. (20) reduces to the known result that the average gap

$$\Delta_0^2(t) = (1-5a^2)(1-t) \frac{8(\pi T_c)^2}{7\zeta(3)}, \quad (21)$$

with $\Delta_1(t) = \Delta_0(t)(1+a)$ and $\Delta_2(t) = \Delta_0(t)(1-a)$. For the isotropic case (equivalent to one band) $a^2 = 0$ and Eq. (20) reduces to

$$\Delta^2(t) = (1-t) \frac{8(\pi T_c)^2}{7\zeta(3)} - \frac{2}{3} q_s^2 v_F^{*2}, \quad (22)$$

as is well known.

The expression for the contribution to the current from the i 'th band is given in renormalized BCS by Eq. (11). Expanding near $T = T_c$ for small q_s and Δ gives

$$j_{si}(t) = \frac{n_i e}{m_i v_{Fi}} \frac{7\zeta(3)}{4(\pi T_c)^2} \Delta_i^2(t) v_{Fi}^* q_s. \quad (23)$$

The total current is the sum over both bands and can be written as

$$j_s(t) = \left[\frac{n_1}{m_1^*} \Delta_1^2(t) + \frac{n_2}{m_2^*} \Delta_2^2(t) \right] \frac{7\zeta(3)}{4(\pi T_c)^2} e q_s, \quad (24)$$

where $m_i^* = m_i(1 + \lambda_{ii} + \lambda_{ij})$. Substituting into Eq. (24) the new expression from Eq. (17) (and equivalent for $1 \leftrightarrow 2$) for $\Delta_1^2(t)$, one obtains two terms. The first proportional to q_s and the second to q_s^3 . This gives the total current j_s as a function of q_s . The critical current $j_c(t)$ is obtained as the maximum of $j_s(t, q_s)$ as a function of q_s . After finding the extremum value of q_s , we obtain for $j_c(t)$

$$j_c(t) = \frac{8e\pi T_c}{3\sqrt{7\zeta(3)}} (1-t)^{3/2} \times \left[\frac{n_1}{m_1^*} \frac{1}{\chi_1} + \frac{n_2}{m_2^*} \frac{1}{\chi_2} \right]^{3/2} \left[\frac{n_1}{m_1^*} \frac{1}{\chi_1'} + \frac{n_2}{m_2^*} \frac{1}{\chi_2'} \right]^{-1/2} \quad (25)$$

We first note that the standard Ginzburg-Landau $(1-t)^{3/2}$ temperature dependence of the critical current remains unmodified in the two-band model. As a first check on our expression in Eq. (25), we can recover the known one-band result when both bands are assumed to be identical by taking $\lambda_{ij} = \lambda/2$, $v_{F1} = v_{F2}$, and the value of $n_1 = n_2 = n_T/2$. Here n_T is the total electron density per unit volume equal to the sum $n_1 + n_2$. We obtain the standard Ginzburg-Landau result[9]:

$$j_c(t) = \frac{8en_T}{3mv_F} \left(\frac{\pi T_c}{\sqrt{7\zeta(3)}} \right) (1-t)^{3/2}. \quad (26)$$

Note that all effective mass renormalization $(1+\lambda)$ factors have cancelled in Eq. (26). Applying the separable gap anisotropy model to Eq. (25) leads to a modification of Eq. (26) by a multiplicative factor of $(1-4a^2)$. This gap anisotropy will decrease $j_c(t)$ over its value for $a = 0$.

Decoupled bands give the usual expression of Eq. (26) since the second band makes no contribution near $T = T_c$, but now n , m , and v_F are those of the first band only. In the general case, we need to return to Eq. (25) which tells us how material parameters affect the slope of $j_c(t)^{2/3}$ which varies linearly with $(1 - t)$ near T_c . If we normalize the current, as we will in the next section, to a slope of negative one near T_c , this will mean that the current at $T = 0$ will vary with material parameters in contrast to the one-band BCS curve for which it is a universal number for the clean limit case that we are discussing here.

A well known result of Ginzburg-Landau theory is that near T_c , $H_c(t)/\lambda_L(t) = (3\pi\sqrt{6}/c)j_c(t)$, where $H_c(t)$ is the thermodynamic critical field and $\lambda_L(t)$ is the London penetration depth, both for the case of zero current. In a previous paper[2], we have given expressions for $H_c(t)$ and $1/\lambda_L^2(t)$ as $t \rightarrow 1$. Using these with Eq. (25), we arrive at the expression relating the two-band H_c , λ_L and j_c :

$$\frac{H_c(t)}{\lambda_L(t)j_c(t)} = \frac{3\pi\sqrt{6}}{c}J, \quad (27)$$

where c is the velocity of light and J is a complicated material-dependent parameter. It is given by

$$J = \sqrt{\left(\frac{N_1^*v_{F1}^{*2}}{\chi_1'} + \frac{N_2^*v_{F2}^{*2}}{\chi_2'}\right)\left(\frac{N_1^*}{\chi_1^2} + \frac{N_2^*}{\chi_2^2}\right)\left[\frac{N_1^*v_{F1}^{*2}}{\chi_1} + \frac{N_2^*v_{F2}^{*2}}{\chi_2}\right]} \quad (28)$$

where we have found it convenient to change from electron density n_i , to density of states at the Fermi surface $N_i(0) \equiv N_i$. This modifies the usual Ginzburg-Landau relation by a constant factor. For the decoupled case where $1/\chi_2 = 1/\chi_2' = 0$, $1/\chi_1' = v_{F1}^{*2}$, and $1/\chi_1 = 1$, J becomes equal to 1. There is no change in the Ginzburg-Landau relation and this makes sense since near $t = 1$ we are dealing with the single band (the first one). For the isotropic gap case, where $\lambda_{ij} = \lambda/2$ for any (i, j) , from Eqs. (18) and (19) we obtain $1/\chi_1 = 1/\chi_2 = 1$ and $1/\chi_1' = 1/\chi_2' = (v_{F1}^{*2} + v_{F2}^{*2})/2$, the average of the squares of the Fermi velocities in the two bands, which gives

$$J = \sqrt{\frac{(N_1 + N_2)(v_{F1}^{*2} + v_{F2}^{*2})}{2(N_1v_{F1}^{*2} + N_2v_{F2}^{*2})}}. \quad (29)$$

For identical bands, this expression gives 1, as it must. This also holds if either the two Fermi velocities are the same or the two density of states match, but not if both parameters for one band differ from those of the other band. We see that, in general, J can be either greater or less than one and the Ginzburg-Landau relation ceases to hold.

For identical bands but with gap anisotropy in the separable small anisotropy a^2 model, $1/\chi_1' = v_F^2/\chi_1$ and $1/\chi_2' = v_F^2/\chi_2$, with $1/\chi_1 = (1 + a)^2(1 - 5a^2)$ and $1/\chi_2 = (1 - a)^2(1 - 5a^2)$ which gives $J = 1$ to order a^2 . This result is expected since, as is well known, the

a^2 anisotropy correction to $H_c(t)$ and $1/\lambda_L(t)$ are both of the form $(1 - 2a^2)$ which gives a factor of $(1 - 4a^2)$ in the ratio $H_c(t)/\lambda_L(t)$. This agrees perfectly with the anisotropy factor we derived earlier for $j_c(t)$. Thus, in this case, the Ginzburg-Landau relation will hold.

We wish to comment on the use of the Ginzburg-Landau relation $H_c(t)/\lambda_L(t) = (3\pi\sqrt{6}/c)j_c(t)$ for comparison with data at all temperatures, which is done by substituting two-fluid model forms for $H_c(t)$ and $\lambda_L(t)$. The Ginzburg-Landau result should only hold near T_c and indeed we find that when we form the ratio of $H_c(t)/\lambda_L(t)$ using the $H_c(t)$ and $\lambda_L(t)$ from the full Eliashberg procedure, the resulting $j_c(t)$ curve rapidly deviates from the Eliashberg calculated $j_c(t)$. The results of using such a phenomenological procedure can give curves which are lower or higher than the true result, and will not even reproduce the qualitative feature of a kink in the $j_c(t)$ that we have found in the two-band calculation. We conclude that the Ginzburg-Landau procedure should only be used near T_c as is appropriate to its derivation and no reliable use can be made of it phenomenologically for lower temperatures.

B. RBCS for $T = 0$

We now turn to low temperature and examine results of RBCS at $T = 0$. At zero temperature, the renormalized BCS gap equation (8) takes on the form

$$\Delta_1 = \bar{\lambda}_{11}\Delta_1\mathcal{G}(\Delta_1, \bar{s}_1) + \bar{\lambda}_{12}\Delta_2\mathcal{G}(\Delta_2, \bar{s}_2) \quad (30)$$

$$\Delta_2 = \bar{\lambda}_{21}\Delta_1\mathcal{G}(\Delta_1, \bar{s}_1) + \bar{\lambda}_{22}\Delta_2\mathcal{G}(\Delta_2, \bar{s}_2) \quad (31)$$

where the barred quantities are renormalized by the factor of Z_i of Eq. (10) and

$$\begin{aligned} \mathcal{G}(\Delta, \bar{s}) &= \ln\left(\frac{2\omega_D}{\Delta}\right), \quad \text{for } \bar{s} < \Delta \\ &= \ln\left(\frac{2\omega_D}{\Delta}\right) - \cosh^{-1}\left(\frac{\bar{s}}{\Delta}\right) + \sqrt{1 - \left(\frac{\Delta}{\bar{s}}\right)^2}, \\ &\quad \text{for } \bar{s} > \Delta \end{aligned} \quad (32)$$

These equations need to be solved numerically. Results are shown in the four lefthand panels of Fig. 1. The top frame is for $\lambda_{11} = 1$, $\lambda_{22} = 0.5$, $\lambda_{21} = \lambda_{12} = 0.01$ (nearly decoupled bands) and $v_{F1} = v_{F2}$. Because λ_{12} is so small, the larger gap Δ_1 exhibits the known behavior as a function of $q_s v_{F1}^*/\Delta_{10}$ of a one-band s-wave superconductor[7] with a small modification. In one-band, the gap would be unchanged until $q_s v_{F1}^*/\Delta_{10} \simeq 1.0$ at which point it would begin a sharp drop toward zero which is reached at $q_s v_{F1}^*/\Delta_{10} \simeq 1.35$. Here, the same behavior occurs but there is a very slight drop from the $q_s = 0$ value of Δ at $q_s v_{F2}^*/\Delta_{20} \simeq 1.0$ due to the coupling to the second band. The lower gap behaves differently. It retains its $q_s = 0$ value until $q_s v_{F2}^*/\Delta_{20} \simeq 1.0$ at which point it also begins a rapid drop but retains a small finite value until the point when $\Delta_1 = 0$. This small tail

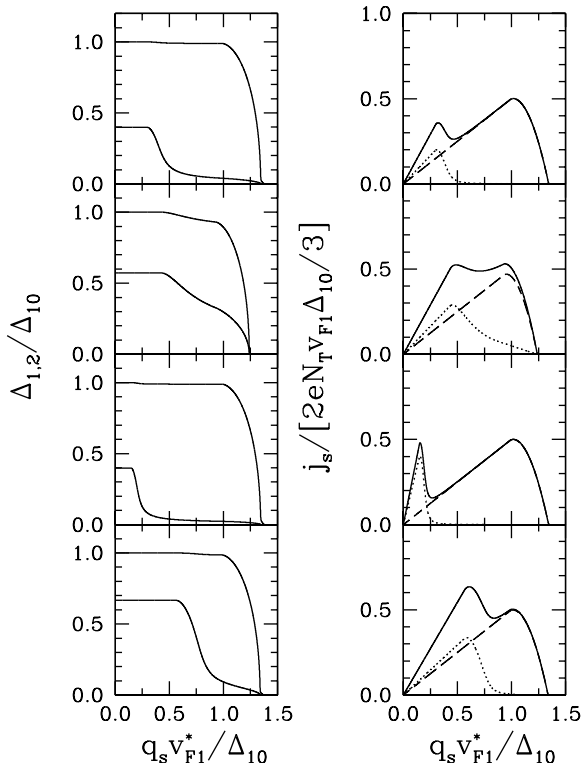


FIG. 1: Renormalized BCS calculations for $T=0$ showing, on the left, the upper and lower gaps as a function of the superfluid momentum q_s . The top frame is for $\lambda_{11} = 1.0$, $\lambda_{22} = 0.5$ and $\lambda_{12} = \lambda_{21} = 0.01$, with $v_{F2}/v_{F1} = 1.0$. In the second, the interband coupling $\lambda_{12} = \lambda_{21}$ has been changed to 0.1. In the third frame, the parameters are the same as for the first frame but now $v_{F2}/v_{F1} = 2.0$. Finally, for the bottom frame, the parameters are the same as for the top frame but now $\lambda_{22} = 0.7$. On the right is shown the total superfluid current density j_s for each case (solid line) and those components for the first band j_{s1} (dashed line) and the second band j_{s2} (dotted line).

is due to the coupling $\lambda_{12} = \lambda_{21}$ which guarantees that the second gap is nonzero, although it can be very small, as long as the first gap is finite. In the second frame $\lambda_{12} = \lambda_{21}$ has been increased to 0.1. This results in a considerable integration of the two gaps. At $q_s = 0$ the lower gap ratio Δ_2/Δ_{10} has increased from the 0.4 value of the top frame to 0.57. More significantly for the present paper, as q_s increases both gaps retain their $q_s = 0$ value until $q_s v_{F2}^*/\Delta_2 \simeq 1.0$, which is the point at which the second gap starts to decrease, but this drop is not as fast as in the top frame because of the large interband coupling. At the same point as the second gap starts to decrease, the first is also reduced but by much less. Beyond $q_s v_{F1}^*/\Delta_{10} \simeq 1.0$ both gaps drop sharply as expected and reach zero together at $q_s v_{F1}^*/\Delta_{10} \simeq 1.27$, a value which is smaller than the one band value of 1.35. This shift in zero along the horizontal axis is also accompanied by a shift to the left, relative to the decoupled case, of the inflection points just described, but these shifts are small. These are signatures of the two-band nature of our system. In the third frame of Fig. 1 (left-

hand side), we have retained $\lambda_{12} = \lambda_{21} = 0.01$ but now have increased the ratio v_{F2}/v_{F1} to 2.0 instead of 1.0. This has the effect of reducing the region of q_s in which the second gap remains constant at its $q_s = 0$ value and is due to the increase in v_{F2}^* . For the last frame, we have kept the parameters as in the first frame but have increased λ_{22} to a value of 0.7. This has the effect of increasing the $q_s = 0$ value of the second gap and also increasing the range over which it stays constant. Additionally, the tail beyond $q_s v_{F2}^*/\Delta_{20} \simeq 1.0$ is not as small as it is in the top frame due to less gap anisotropy.

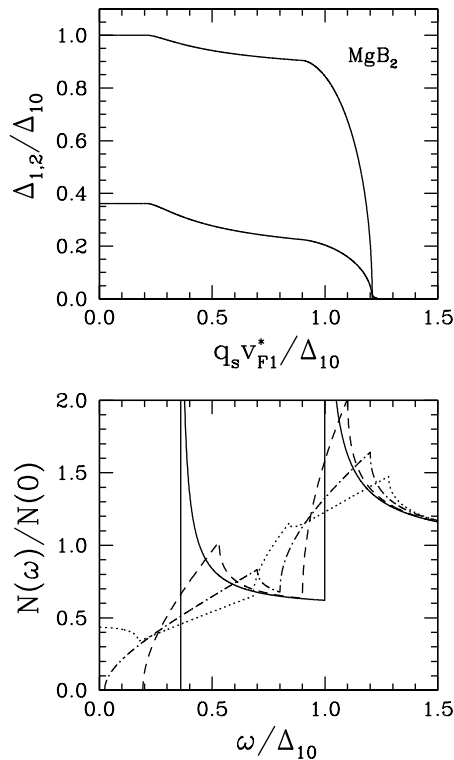


FIG. 2: Upper frame: The two gaps for MgB_2 parameters, calculated at $T=0$ for in the renormalized BCS theory, shown as a function of the superfluid momentum q_s . Lower frame: The density of states $N(\omega)/N(0)$ as a function of ω is shown for several values of $q_s v_{F1}^*/\Delta_{10} = 0.0001$ (solid), 0.1 (dashed), 0.2 (dot-dashed) and 0.3 (dotted).

In renormalized BCS, Eq. (11) for the partial current can be evaluated analytically at zero temperature to obtain

$$\begin{aligned}
 j_{si}(0) &= \frac{en_i}{1 + \lambda_{ii} + \lambda_{ij}} q_s, & \text{for } \frac{\bar{s}_i}{\Delta_{i0}} < 1 & \quad (34) \\
 &= \frac{en_i}{1 + \lambda_{ii} + \lambda_{ij}} q_s \left[1 - \left[1 - \left(\frac{\Delta_{i0}}{\bar{s}_i} \right)^2 \right]^{3/2} \right], & & \\
 & & \text{for } \frac{\bar{s}_i}{\Delta_{i0}} > 1 & \quad (35)
 \end{aligned}$$

Results for the current are presented in the righthand side frames of Fig. 1 for the four sets of parameters considered on the lefthand side. In all cases, the dotted lines give the results for the partial contribution to the current

coming from the second band and the dashed for those from the first. The sum of the two partial contributions is the solid curve. A first feature to note is that for the three frames for which $\lambda_{12} = \lambda_{21} = 0.01$ (nearly decoupled), the dashed curves are essentially identical. The straight line segment has slope 0.5 in our units and the zero is very nearly at $q_s v_{F1}^*/\Delta_{10} = 1.35$ as in the one-band case. Note that on the vertical axis, we have used the total electronic density of states $N_T = N_1(0) + N_2(0)$ with $N_1(0) = N_2(0)$. If we had used only $N_1(0)$ then the slope of the straight line segment would have been 1 which corresponds to what is expected in the one-band case. A second point to note is that increasing $\lambda_{12} = \lambda_{21}$ to 0.1 as in the second frame from the top has not had a large effect on the partial current from the first band except to reduce somewhat the value of q_s at which the current goes to zero. This is accompanied by a small shift to the left in the position of the peak and a small reduction in its height. By contrast, the effect of the parameter changes are much more significant on the dotted curve (the current in the second band). In the top frame, the slope of the straight line portion of the dotted curve is a little larger than 0.5 because of the renormalization factors on v_{F2}^* relative to v_{F1}^* . More significantly the partial current starts to deviate from linearity at $q_s v_{F2}^*/\Delta_{20} \simeq 1$ at which point it drops rapidly towards zero but remains finite (although small) until the current in the first band has reached zero. This also applies to the third frame although in that case the current in the second band has been increased in value because of the increase in v_{F2} by a factor of two. In all cases the total current (solid curve) exhibits two peaks. The peak arising at lower values of q_s has a significant contribution from both bands while the other peak at higher values of q_s is due almost entirely to the partial current of the first band when $\lambda_{12} = \lambda_{21}$ is very small. On the other hand, when there is more integration of the two systems (second frame from top) both bands can make a significant contribution. In the top three frames, the first peak is lower than the second while in the fourth frame, the opposite holds. The height of the first peak can be made higher by increasing the value of v_{F2} as in the third frame compared with the first (or equivalently, increasing N_2/N_1 as the density of states enters in combination with v_F and so will have a similar effect, which is redundant to discuss here) or by increasing λ_{22} as in the fourth, again compared with the first. It can also be increased by increasing the offdiagonal coupling as in the second frame. When this is done, however, the contribution of the second band to the total current in the second peak is also increased. Finally we note that the peak heights in the two middle frames are only very slightly different and the lower q_s peak could be made to be the highest through a small tuning of the parameters. As the highest peak determines the value of j_c , this transfer from one peak to the other by varying parameters is very interesting and will produce nonstandard effects at finite temperature.

C. RBCS at T=0 for MgB₂

Before leaving our discussion of RBCS at $T = 0$, it is of interest to consider the specific case of MgB₂ now well-established to be a two-band electron-phonon superconductor. Microscopic parameters have been calculated from extensions of bandstructure calculations to obtain the electron-phonon spectral densities. The Coulomb repulsion parameters that enter the gap equations (5) and (6) are also known. The parameters are $\lambda_{\sigma\sigma} = 1.017$, $\lambda_{\pi\pi} = 0.448$, $\lambda_{\sigma\pi} = 0.213$, $\lambda_{\pi\sigma} = 0.155$, $\mu_{\sigma\sigma}^* = 0.210$, $\mu_{\pi\pi}^* = 0.172$, $\mu_{\sigma\pi}^* = 0.095$, $\mu_{\pi\sigma}^* = 0.069$, with $\omega_c = 750$ meV. The ratio of the two density of states $N_\pi(0)/N_\sigma(0) = 1.37$ and of the Fermi velocities $v_{F\pi}/v_{F\sigma} = 1.2$. To switch to our notation, $(\sigma, \pi) = (1, 2)$. We start with RBCS results. In the top frame of Fig. 2, we show the dependence of Δ_1 and Δ_2 normalized to Δ_{10} as a function of $q_s v_{F1}^*/\Delta_{10}$. On comparison with some of the results of Fig. 1, we note that MgB₂ shows considerable integration of the two bands and also both gaps become zero at $q_s v_{F1}^*/\Delta_{10} \simeq 1.2$ which is considerably reduced from the one-band BCS value.

An interesting quantity that could be measured is the quasiparticle density of states $N(\omega)/N(0)$ in the presence of a current, which was first examined for one-band s-wave superconductors by Fulde[8]. Such measurements have recently been reported for Pb in Ref. [24]. For each band separately

$$N_i(\omega) = \frac{N_i(0)}{2\bar{s}_i} \Re e \left[\frac{\omega + \bar{s}_i}{|\omega + \bar{s}_i|} \sqrt{(\omega + \bar{s}_i)^2 - \Delta_i^2} - \frac{\omega - \bar{s}_i}{|\omega - \bar{s}_i|} \sqrt{(\omega - \bar{s}_i)^2 - \Delta_i^2} \right] \quad (36)$$

with $N(\omega) = N_1(\omega) + N_2(\omega)$. In the bottom frame of Fig. 2, we give results for $N(\omega)/N_T(0)$ as a function of ω/Δ_{10} for various values of q_s as indicated in the figure. The solid curve is essentially the zero current limit and shows the expected superposition of two BCS quasiparticle density of states with square root singularities at the two gaps. As the current is increased in the linear region only (cross-referencing with the upper frame of Fig. 3 which shows j_s for MgB₂), the singular structure is smeared and the gap region fills as does the region between the two gaps. Gapless behavior appears at a value of q_s near the first peak in the total current due to the density of states in the small band going gapless. This is in contrast to what is found in a one-band s-wave superconductor[8] where the gapless behavior occurs at the critical current.

The superfluid current j_s versus q_s for the RBCS calculation with MgB₂ parameters is plotted in the upper frame of Fig. 3. The line types are defined in the same way as for the j_s curves in Fig. 1. We note that this graph is very similar to that shown in the second frame (righthand side) of Fig. 1, where it has been discussed in relation to other cases. As in that graph, the peak in the total current seen at low q_s is lower than the one at

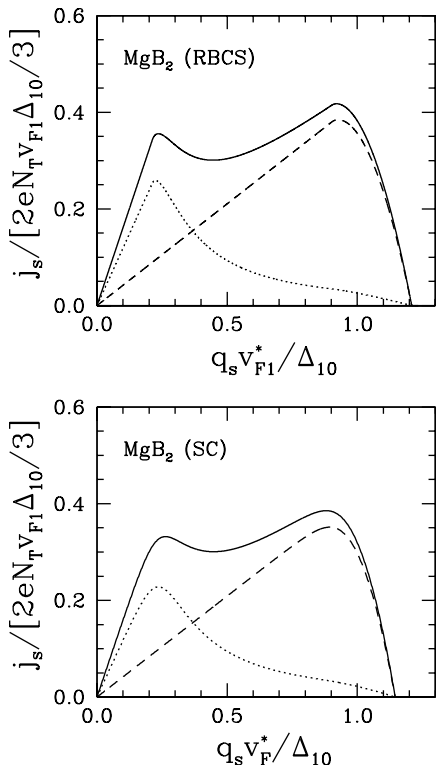


FIG. 3: The current j_s as a function of q_s calculated for the MgB₂ parameters. Shown are the component contributions of the currents for the first and second bands (dashed and dotted curves, respectively) and the total current (solid curve). The upper frame shows the calculation for $T = 0$ RBCS and the bottom frame shows the curves calculated in Eliashberg theory for $T/T_c = 0.1$.

higher q_s , so that this second peak determines the critical current. It is of considerable interest to compare these renormalized BCS results with those from full Eliashberg calculations based on the $\alpha_{ij}^2 F(\omega)$ spectra given in Ref. [21]. Very similar values of the parameters can also be found in Ref. [22]. Such results are presented in the lower frame of Fig. 3. There are several differences that are worthy of note. The full Eliashberg results are at $T/T_c = 0.1$ and the RBCS are for $T = 0$. This difference in temperature is small and is not expected to lead to any significant differences. Examination of the partial currents shows that the dashed curves are almost the same in both plots except that strong coupling effects have shifted the point of zero current to a slightly smaller value of q_s . This is accompanied by a shift to the left of the position of the peak, a reduction in its height and an increase in the rounding, all small effects. These differences are seen to be slightly more prominent in the dotted curve. This shows that RBCS can be used with confidence as a first approximation. However, from this point on, we will consider only Eliashberg results as we have available to us the electron-phonon spectral functions and we wish to consider the full effects of temperature and impurities.

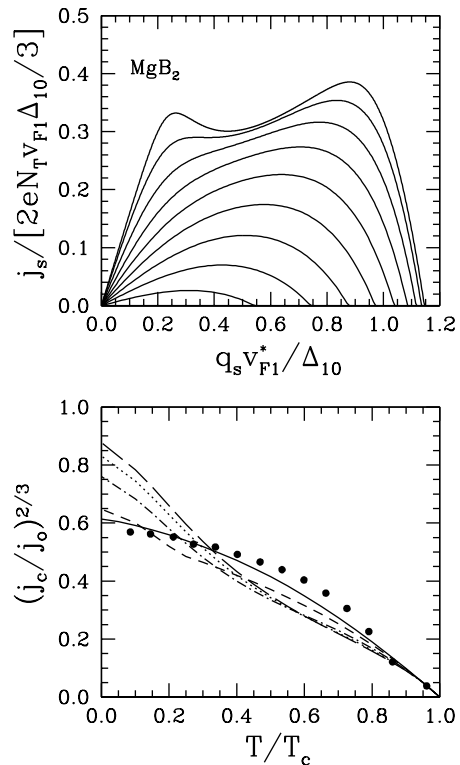


FIG. 4: Upper frame: The temperature evolution of the j_s versus q_s for MgB₂ calculated in Eliashberg theory. From top to bottom, the temperatures range from $T/T_c = 0.1$ to 0.9 in steps of 0.1 . Lower frame: The critical current plotted as $j_c^{2/3}$ versus T/T_c for MgB₂ with varying v_{F2}/v_{F1} ratio equal to 1.2 (solid curve - corresponding to the set of curves shown in the upper frame), 2 (short dashed), 3 (dot-dashed), 4 (dotted), and 5 (long-dashed). The solid dots are the data for MgB₂ taken from Kunchur[16]. The data appears to be in good agreement with the solid curve which corresponds to the standard set of parameters given for MgB₂ in the literature.

IV. ELIASHBERG CALCULATIONS FOR FINITE T AND IMPURITIES

At the end of the last section, we showed a comparison between RBCS and Eliashberg theory (Fig. 3). Given that the electron-phonon spectral functions for MgB₂ are available, it is appropriate to work with the full theory for j_c as a function of temperature and impurity scattering. We begin with a consideration of temperature effects. In the upper frame of Fig. 4, we show the current $j_s(T)$ normalized by $2eN_T v_{F1} \Delta_{10} / 3$ as a function of $q_s v_{F1}^* / \Delta_{10}$ for nine values of temperature from $T/T_c = 0.1$ to 0.9 in steps of 0.1 . The parameters used are those appropriate to MgB₂ with the upper curve reproduced from the bottom frame of Fig. 3. As the temperature is increased, the peak with larger value of q_s remains the highest and therefore determines the critical current given as the solid curve in the lower frame. Here, j_c has been normalized by j_0 so that the slope at $t = 1$ is negative one by arrangement for the typical critical current plot of $j_c^{2/3}$, which is designed to bring out the Ginzburg-Landau be-

havior near T_c . We see a smooth (concave downward) increase in $j_c(t)$ as t is reduced. The value of the critical current at $t = 0$ is ~ 0.61 . This is lower than the one-band BCS value of 0.72. This reduction could reflect the two-band nature of MgB₂ as well as strong coupling corrections[2, 12] due to our use of the full Eliashberg equations (5) and (6) to calculate the current given by Eq. (4). However, reference to the lower frame of Fig. 3 shows that the second band contributes only about 10% to the total critical current at $T = 0$ and this remains true at T_c . Consequently, this curve is very nearly the single band result and deviates from the classical BCS curve almost entirely because of retardation effects. Also shown is the data of Kunchur[16], plotted as solid dots. There is good agreement between the data and the solid curve which is quite remarkable as the calculation has no free parameters, in principle, as they are all given in the literature. Including impurity scattering has an effect on the temperature dependence of $j_c(t)$, as we will discuss later in relation to Fig. 7. Unfortunately, information on the individual intraband scattering rates in these films for π and σ bands, separately, is not available to us. Including some impurity scattering in the π band would further improve the agreement with experiment. The other critical current curves in Fig. 4 are for different ratios of v_{F2}/v_{F1} as indicated in the figure caption. In addition to allowing for some uncertainty in the reported v_F values in the literature, this also mimics the possibility of currents associated with the c-axis where the σ -band is known to have a much smaller v_F than the π -band. Likewise, we have not included the details of the full Fermi surface average in the expression for the current, however, it is known that the σ -band is quasi-two-dimensional as opposed to the more three-dimensional π -band. Dahm and Scalapino[18] find significant geometrical corrections associated with such averaging which could also accentuate the difference between the two bands. This may also be approximately captured by our use of different v_F ratios. All the curves are normalized to have a slope of negative one at $t = 1$. As v_{F2} is increased, the normalized critical current at zero temperature increases and can become considerably larger than its one-band BCS value. There is also a change in the temperature variation of the curves, the dashed curve shows a clear kink around $t \simeq 0.25$ while the long-dashed curve shows concave upward behavior at intermediate temperatures. This can be understood better when the pattern of behavior shown in Fig. 5 is considered. The top frame gives the temperature evolution for the case $v_{F2}/v_{F1} = 2$ and the bottom is for a ratio of 4. The notation is as for the top frame of Fig. 4 and for the same nine reduced temperatures. In the top frame, it is the peak at lower q_s which determines the critical current at $t = 0$ while at higher t , it is the peak with higher q_s . This crossover occurs between $t = 0.2$ and $t = 0.3$ and leads to the kink seen in the dashed curve of Fig. 4 (lower frame). If we look at the individual contributions from each band (not shown here) to the total current, we find that at $T = 0$ it is

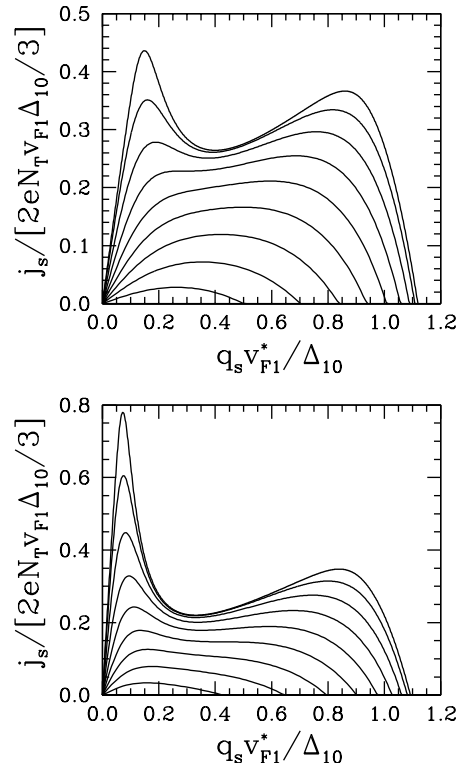


FIG. 5: The temperature evolution of the j_s versus q_s curves for MgB₂ calculated in Eliashberg theory. From top to bottom, the temperatures range from $T/T_c = 0.1$ to 0.9 in steps of 0.1. The upper frame is for a v_{F2}/v_{F1} ratio equal to 2 and the lower frame is for a ratio of 4.

the second band which makes the dominant contribution because of its large value of v_F but near T_c this contribution has decayed sufficiently that it only makes a 30% contribution to the total.

In the lower frame of Fig. 5, the peak at smaller value of q_s has greatly increased in magnitude over its value in the top frame. It has also moved to a lower value of q_s as expected from Fig. 1. However, now there is no crossover from smaller to larger q_s peak and hence no kink. Nevertheless, the dotted curve is very different from a one-band BCS variation. We can understand better how this can arise by once more looking at the partial contribution to the critical current from each band. At $T = 0$ it is the second band which dominates while at T_c it accounts only for 2/3 of the total with the remaining 1/3 contribution from band one. This difference in admixture of the two bands with temperature is seen to be enough to cause an upward curvature in the dotted curve at intermediate temperatures as well as to increase the value of the normalized critical current at $T = 0$ to a value considerably larger than the BCS value of 0.72. Increasing v_{F2} further as in the long-dashed curve of the lower frame of Fig. 4 increases the $T = 0$ value even further as the peak at lower q_s value becomes even more prominent. Details of the temperature variation of the critical current clearly depend on details of the microscopic parameters of the two bands involved, such as values of λ_{ij} , N_i , v_{Fi} . For

example, it is possible to shift the kink in $j_c(t)$ to higher values of reduced temperature and to make it sharper by considering other parameter sets. To illustrate this,

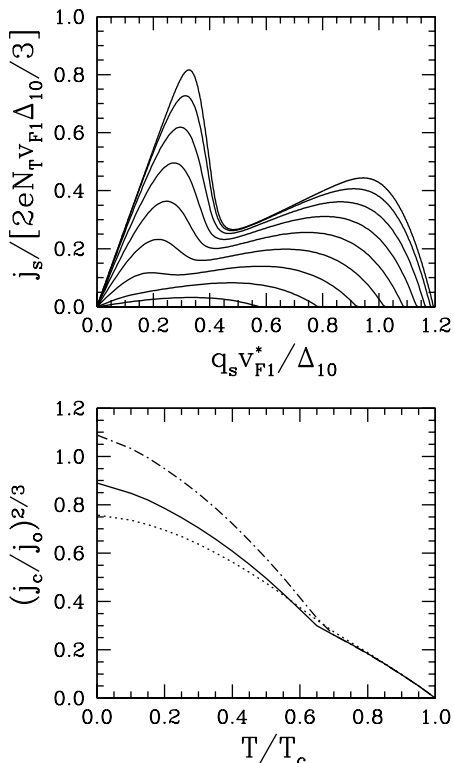


FIG. 6: Upper frame: The temperature evolution of curves for j_s versus q_s for a Lorentzian spectrum with $v_{F2}/v_{F1} = 2$, $\lambda_{11} = 1$, $\lambda_{22} = 0.8$, and $\lambda_{12} = \lambda_{21} = 0.01$. From top to bottom, the temperatures range from $T/T_c = 0.1$ to 0.9 in steps of 0.1 . Lower frame: The critical current as a function of temperature corresponding to the same curves in the upper frame (solid curve) and also for the cases of $v_{F2}/v_{F1} = 1$ (dotted) and 3 (dot-dashed).

in Fig. 6 we show results for a Lorentzian $\alpha_{ij}^2 F(\omega)$ spectrum defined in detail in our previous paper[2]. In this model, $\lambda_{11} = 1$ and we take $\lambda_{22} = 0.8$ to decrease the gap anisotropy as compared with MgB₂. We have also taken $\lambda_{12} = \lambda_{21} = 0.01$ (nearly decoupled bands). The top frame gives the current $j_s(t)$ for the case of $v_{F2}/v_{F1} = 2$, for the nine values of reduced temperature previously chosen. With this v_F ratio, the peak with lower value of q_s remains highest at small t and the crossover of the maximum to the other peak occurs at a reduced temperature between 0.6 and 0.7 . This manifests itself as a sharp kink in the solid curve for j_c (bottom frame) at this same temperature. Also shown in this same frame are results for the critical current when $v_{F2}/v_{F1} = 1$ (dotted) and $v_{F2}/v_{F1} = 3$ (dot-dashed). For the larger value of v_{F2} , the normalized current at $T = 0$ is increased over the $v_{F2}/v_{F1} = 2$ case as expected and for $v_{F2} = v_{F1}$ it is reduced but remains above BCS. In this latter case, the two peaks in the current versus q_s are closer together than they are in the top frame of Fig. 6 and seem to almost merge before the crossover from lower to higher

q_s peak occurs, which means that the kink in the dotted curve can hardly be seen. It is clear that a rich pattern of behavior exists for the current versus q_s at different reduced t in a two-band model. This translates into quite distinct temperature dependence for $j_c(t)$ as compared with the one-band BCS canonical behavior.

Some addition insight into this complicated behavior can be obtained from a consideration of simplified but analytic BCS results in the limiting case of two decoupled, well-separated bands, i.e., for small values of the gap anisotropy $u = \Delta_{20}/\Delta_{10}$. Under this assumption, $1/\chi_1 = 1$, $1/\chi_2 = 0$, $1/\chi'_1 = v_{F1}^{*2}$, and $1/\chi'_2 = 0$ so that the critical current near T_c given by formula (25) reduces to

$$j_c(t) = \frac{16}{9} \frac{e\pi T_c}{\sqrt{7\zeta(3)}} N_1 v_{F1} (1-t)^{3/2}, \quad (37)$$

and is determined entirely by band one, as previously commented upon. As the temperature is lowered, however, two possible circumstances can arise. The critical current can remain determined by the same band (number one) in which case we can write approximately

$$j_c(0) \simeq \frac{n_1 e}{m_1 v_{F1}} \Delta_{10}. \quad (38)$$

A second possibility is that a crossover to the peak at lower q_s value occurs and we have approximately

$$j_c(0) \simeq \left(\frac{n_1}{m_1} + \frac{n_2}{m_2} \right) \frac{e\Delta_{20}}{v_{F2}}. \quad (39)$$

For the first case,

$$\left(\frac{j_c(0)}{j_0} \right)^{2/3} = 0.72 \quad (40)$$

which is the one-band BCS result where we have normalized the critical current in such a way that $j_c^{2/3}$ has a slope of negative one at $t = 1$. This conforms with what we have done in the lower frames of Figs. 4 and 6. For the second case, by assumption, there is a crossover and

$$\left(\frac{j_c(0)}{j_0} \right)^{2/3} = 0.72 \left[\frac{\Delta_{10}}{1.76 T_c} u \left\{ \frac{N_2 v_{F2}}{N_1 v_{F1}} + \frac{v_{F1}}{v_{F2}} \right\} \right]^{2/3}. \quad (41)$$

This simplified approximate formula shows clearly that the anisotropy u on its own reduces the value of $(j_c(0)/j_0)^{2/3}$ below its universal BCS value of 0.72 while a large value of N_2 relative to N_1 or v_{F2} relative to v_{F1} increases it and that this reduced dimensionless quantity is no longer universal. It can depend on the band structure parameters as well as on the gap anisotropy.

Next we consider the effect of impurities on the current. It is instructive to begin by expanding Eq. (4) for $j_s(t)$ to lowest order in q_s . Doing so leads to the well-known and physically expected result that for small superfluid velocity

$$j_s(t) = \sum_{i=1}^2 j_{si} = \sum_{i=1}^2 e n_{si} v_s \quad (42)$$

where n_{si} is the superfluid density of the i 'th band given for a strong coupling superconductor by

$$n_{si} = n_i \left[2\pi T \sum_n \frac{\tilde{\Delta}_i^2(n)}{[\tilde{\omega}_i^2(n) + \tilde{\Delta}_i^2(n)]^{3/2}} \right] \quad (43)$$

In BCS at $T = 0$, this becomes $n_1/(1 + \lambda_{11} + \lambda_{12})$ and $n_2/(1 + \lambda_{22} + \lambda_{21})$ for band 1 and band 2, respectively. The slope of $j_s(t)/e$ as a function of v_s gives $n_{s1} + n_{s2}$ with Eq. (43) valid for any temperature and any impurity content. The impurities enter only through the Eliashberg gap equations (5) and (6). As the temperature is increased, the superfluid density is reduced and so the slope of $j_s(t)$ seen in Figs. 4 to 6 is correspondingly reduced. Impurities also reduce the superfluid density. In BCS, the known result for each of the two bands separately, to lowest order, is

$$n_{si} = \frac{n_i}{1 + \lambda_{ii} + \lambda_{ij}} \frac{1}{1 + \frac{\pi^2 \xi_{0i}}{8l_i}} \quad (44)$$

with $\xi_{0i} = v_{Fi}/(\pi\Delta_{i0})$ and $l_i = v_{Fi}\tau_{ii}$, the coherence length and impurity mean free path in the i 'th band, respectively. This applies to intraband scattering which reduces the initial slope of the partial current coming from each band. Results are presented in Fig. 7, where we also consider the interband case $t_{ij}^+ \neq 0$. In the top frame, we show j_s versus q_s for the reduced temperature $t = 0.1$ in the Lorentzian model used in Fig. 6. The solid curve applies to the pure case and is for comparison. We show only three cases, one where $t_{11}^+ = 2T_{c0}$ (dotted curve), $t_{22}^+ = T_{c0}$ (dashed curve), and $t_{12}^+ = t_{21}^+ = 0.02T_{c0}$, where T_{c0} is the T_c without impurities (in the case of t_{11}^+ and t_{22}^+ , T_c will be unaffected, but not so for interband impurities). Intraband impurities reduce only the partial contribution to the current coming from that band. It reduces its value on the vertical axis and extends the x-axis to higher values of q_s leaving the second band largely unaffected. Of course, since both bands contribute significantly to the total current in the region of the peak corresponding to the smaller value of q_s , its magnitude is reduced even in the dotted curve. On the other hand, for the dashed curve, there is little change in the region of the second peak which is dominated by the first band. By contrast interband impurities modify both bands in a similar fashion. The corresponding critical current as a function of T/T_c is shown in the lower frame. The solid line is the pure case of Fig. 6. As expected, a finite value of t_{11}^+ has reduced the critical current below its value in the pure case at all temperatures, however, when normalized to a slope of magnitude one near T_c , the effect pushes the curve up at low T . A kink remains and the crossover temperature is only slightly shifted toward higher values. For the dashed curve, the significant modifications arise only below the kink temperature. By contrast the main effect of the interband impurities is to wash out the kink structure leaving the rest of the curve largely unaffected (of course the T_c would show a small shift downwards relative to T_{c0} , not shown here).

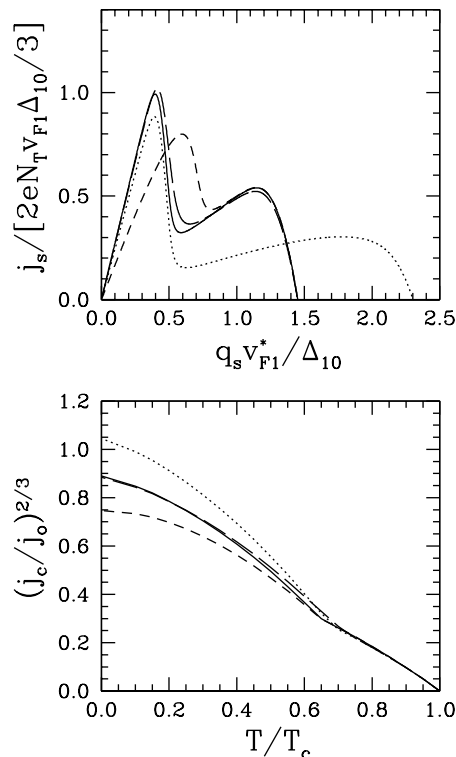


FIG. 7: Upper frame: The superfluid current j_s versus q_s for a Lorentzian spectrum as used in Fig. 6, where the solid curve is repeated from Fig. 6 for $T/T_c = 0.1$ and has a ratio of the two v_F 's equal to 2. The dotted curve is where a scattering rate of $t_{11}^+ = 2T_{c0}$ is now introduced, the short dashed is for $t_{22}^+ = T_{c0}$, and the long-dashed is for $t_{12}^+ = t_{21}^+ = 0.02T_{c0}$. Lower frame: The critical current as a function of temperature corresponding to the parameters for the curves shown in the upper frame.

V. CONCLUSIONS

In conventional one-band s-wave superconductors, the energy gap Δ remains unaffected by the flow of a supercurrent up to a critical value of the superfluid velocity $v_s = q_s/m$ (ie., $v_s^c = \Delta/mv_F$) at which point pairbreaking becomes possible. In this region, the current j_s is linear in v_s with proportionality constant equal to the superfluid density. Beyond this critical value of v_s , the rapid reduction in the gap in addition to a quasiparticle backflow current leads to $j_s = 0$ at $\Delta = 0$. For two nearly decoupled bands, we would expect that the total current to exhibit a two-peak structure as a function of v_s . A first one near the critical value of the superfluid velocity for band two and the other near the larger critical value of v_s corresponding to the first band alone. The first peak has in general a significant contribution from both bands (unless $v_{F2} \gg v_{F1}$) while the second peak could be due mainly to the first band. The relative admixture depends on microscopic parameters such as density of states $N_i(0)$ and Fermi velocities v_{Fi} , as well as gap anisotropy. When v_{F2} is made large as compared to v_{F1} , the first peak moves to lower values of v_s and can

also become larger than the second at low temperature. As the temperature is increased the superfluid density in each band is reduced but that in the second band is more strongly affected because of its smaller gap value. Consequently, since the critical current is determined by the height of the highest peak, one can have a crossover from the first to second peak as T is raised from 0 to T_c and this will reflect itself as a kink in the temperature dependence of the critical current. Such a feature is also found in the dirty limit calculations presented in Ref. [17] for the critical current along the c -axis. When there is a significant interband coupling or the two gaps are close in value (isotropic case) the two peaks in the total current cease to be independent and a rich pattern of behavior emerges for the temperature and impurity dependence of the two peaks. In particular, as the temperature is raised, the first peak can remain the determining peak for j_c up to T_c or it can become the smaller of the two at a crossover temperature which can be increased or decreased through judicious choices of parameters. Another possibility is that the two peaks merge into one or that the second peak is the dominant one at all temperatures. Application to the specific case MgB₂, which involves no adjustable parameters, gives good agreement with the in-plane data of Kunchur[16].

If the resulting critical current $j_c^{2/3}$ is normalized to have slope of negative one as a function of $(1 - t)$ near $t = 1$, the corresponding value of the critical current at $T = 0$ will differ from its classic one-band BCS value of 0.72. Strong coupling effects resulting from our use of the full Eliashberg equations, with appropriate electron-phonon spectral densities describing the electron-phonon interaction, are known[12] to always reduce the normalized value of $j_c(0)$ while two-band effects can reduce or increase it depending on the detailed values of the microscopic parameters involved. In particular, a large value of v_{F2} relative to v_{F1} can lead to values that can be even

larger than one. This is expected for the case of current orientated along the c -axis for the specific parameters representative of MgB₂. In this case, because the σ band (band one in our notation) is nearly two-dimensional, the Fermi velocity of the π band in the c -direction will be much greater than that for the σ band.

The superfluid density in each subband, which determines the initial slope of the linear in v_s regime for the supercurrent, is reduced with the increase in intraband impurity scattering. This fact can be used to manipulate the position along the v_s axis and size of the two peaks in the total current and consequently the temperature dependence of the resulting critical current. Introducing impurities in the first band will reduce the critical current at all temperatures since this band always makes a contribution to the total current. On the other hand, if they are introduced only in the second band, this will leave the critical current largely unaltered around $T = T_c$. Interband impurity scattering affects both bands although not necessarily in exactly the same way and leads to the smoothing out of the kink in $j_c^{2/3}(t)$ versus t when it exists.

In conclusion, we predict a complex pattern of behavior for the total current as a function of v_s , temperature and impurity content which can be used to restrict further the values of the microscopic parameters involved in two-band superconductors, such as MgB₂.

Acknowledgments

EJN acknowledges funding from NSERC, the Government of Ontario (PREA), and the University of Guelph. JPC acknowledges support from NSERC and the CIAR. This research was supported in part by the National Science Foundation under Grant No. PHY99-07949.

-
- [1] J.P. Carbotte, Rev. Mod. Phys. **62**, 1027 (1990).
 - [2] E.J. Nicol and J.P. Carbotte, Phys. Rev. B **71**, 054501 (2005).
 - [3] K.T. Rogers, Ph.D. thesis, University of Illinois, 1960 (unpublished).
 - [4] J. Bardeen, Rev. Mod. Phys. **34**, 667 (1962).
 - [5] R.H. Parameter, *RCA Rev.* **23**, 323, (1962); R.H. Parameter, and L.J. Berton, *RCA Rev.* **25**, 596, (1964)
 - [6] K. Maki, Progr. Theoret. Phys. (Kyoto) **29**, 10 and 333 (1963).
 - [7] K. Maki, in Superconductivity, edited by R.D. Parks (Dekker, New York, 1969), p.1035.
 - [8] P. Fulde, Phys. Rev. **137**, A783 (1965).
 - [9] M.Y. Kupriyanov and V.F. Lukichev, Sov. J. Low Temp. Phys. **6**, 210 (1980).
 - [10] M. Tinkham, *Introduction to Superconductivity* (McGraw-Hill, New York, 1996).
 - [11] T.R. Lemberger and L. Coffey, Phys. Rev. B **38**, 7058 (1988).
 - [12] E.J. Nicol and J.P. Carbotte, Phys. Rev. B **43**, 10210 (1991).
 - [13] D. Zhang, C.S. Ting, and C.-R. Hu, Phys. Rev. B **70**, 172508 (2004).
 - [14] I. Khavkine, H.Y. Kee, and K. Maki, Phys. Rev. B **70**, 184521 (2004).
 - [15] H.Y. Kee, Y.B. Kim, and K. Maki, Phys. Rev. B **70**, 052505 (2004).
 - [16] M.N. Kunchur, cond-mat/0409402; M.N. Kunchur, S.I. Lee, W.N. Kang, Phys. Rev. B **68**, 064516 (2003).
 - [17] A.E. Koshelev and A.A. Golubov, Phys. Rev. Lett. **92**, 107008 (2004).
 - [18] T. Dahm and D.J. Scalapino, cond-mat/0409571
 - [19] See for example, I. Vekhter, P.J. Hirschfeld, and E.J. Nicol, Phys. Rev. B **64**, 064513 (2001).
 - [20] D. Xu, S.K. Yip, and J.A. Sauls, Phys. Rev. B **51**, 16233 (1995).
 - [21] A.A. Golubov, J. Kortus, O.V. Dolgov, O. Jepsen, Y. Kong, O.K. Andersen, B.J. Gibson, K. Ahn, and R.K.

- Kremer, J. Phys.: Condens. Matter **14**, 1353 (2002).
- [22] H.J. Choi, D. Roundy, H. Sun, M.L. Cohen, and S.G. Louie, Nature (London) **418**, 758 (2002).
- [23] H.G. Zarate and J.P. Carbotte, Phys. Rev. B **27**, 194 (1983) and *Anisotropy Effects in Superconductors* edited by H. Webber (Plenum Press, New York, 1977).
- [24] A. Anthore, H. Pothier, and D. Esteve, Phys. Rev. Lett. **90**, 127001 (2003).